Vitamin C inhibits SARS coronavirus-2 main protease essential for viral replication

Tek Narsingh Malla[1&], Suraj Pandey[1&], Ishwor Poudyal[1], Luis Aldama[2], Dennis Feliz[2, 3], Moraima Noda[2], George N. Phillips Jr.[4], Emina A. Stojković[2*], Marius Schmidt[1*]

[1]Department of Physics, University of Wisconsin Milwaukee, Milwaukee, WI 53211 USA
[2]Department of Biology, Northeastern Illinois University, Chicago, IL 60625 USA
[3]Department of Chemistry, Northeastern Illinois University, Chicago, IL 60625 USA
[4]Department of BioSciences, Rice University, Houston, TX 77005 USA
[&]contributed equally
*corresponding authors

Abstract

There is an urgent need for anti-viral agents that treat and/or prevent Covid-19 caused by SARS-Coronavirus (CoV-2) infections. The replication of the SARS CoV-2 is dependent on the activity of two cysteine proteases, a papain-like protease, PL-pro, and the 3C-like protease known as main protease Mpro or 3CLpro. The shortest and the safest path to clinical use is the repurposing of drugs with binding affinity to PLpro or 3CLpro that have an established safety profile in humans. Several studies have reported crystal structures of SARS-CoV-2 main protease in complex with FDA approved drugs such as those used in treatment of hepatitis C. Here, we report the crystal structure of 3CLpro in complex Vitamin C (L-ascorbate) bound to the protein's active site at 2.5 Ångstrom resolution. We also demonstrate that L-ascorbate inhibits the 3CLpro *in vitro* at mmol/L concentrations. The crystal structure of the Vitamin C 3CLpro complex may aid future studies on the effect of Vitamin C not only on the coronavirus main protease but on related proteases of other infectious viruses. Since ascorbate is readily available, as an over-the-counter vitamin supplement, our results have the potential for development of a global and inexpensive antiviral treatment.

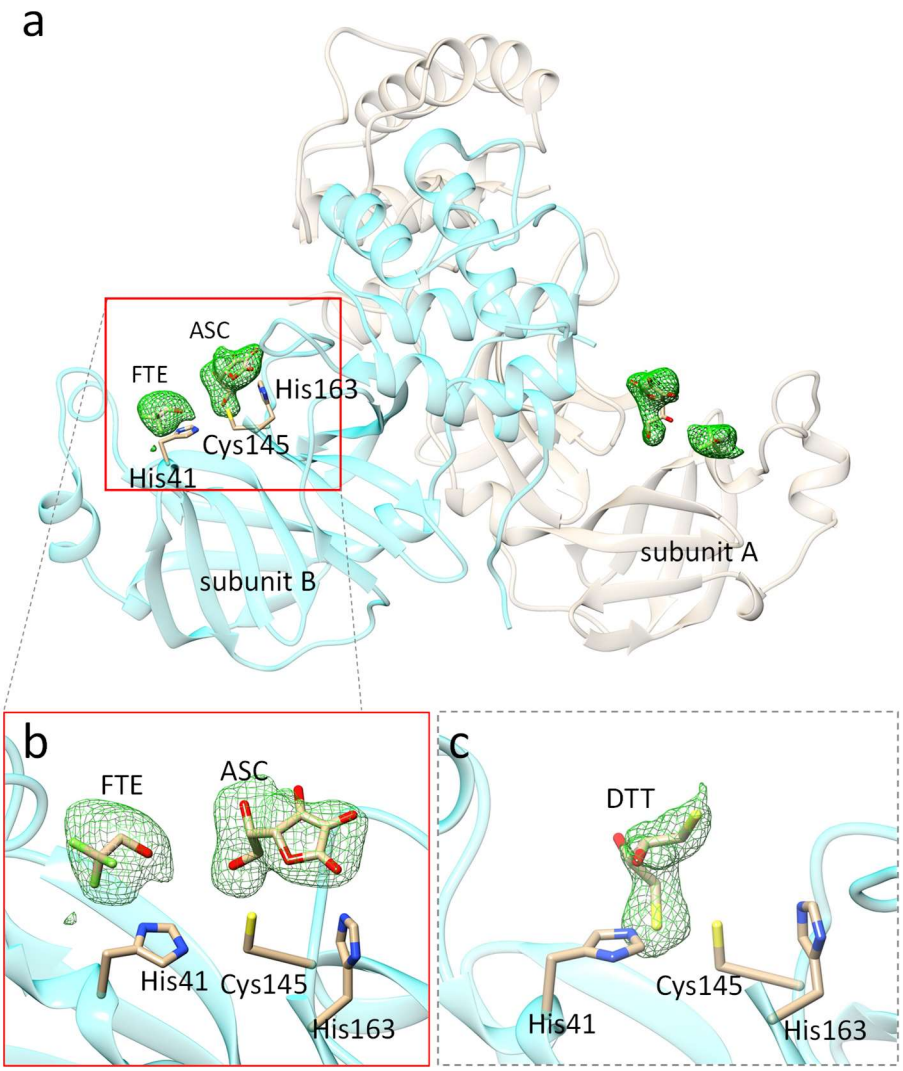

Figure 1. Vitamin C and DTT bound in the active site of SARS CoV-2 3CLpro. (a) The 3CLpro dimer in the asymmetric unit of the orthorhombic crystals soaked with L-ascorbate. Polder difference electron density (Liebschner et al., 2017) in the active sites is shown in green (contour: 2.5 sigma). (b) The L-ascorbate (ASC) in subunit B. The ASC interacts with the catalytic Cys-145 and is stabilized by a hydrogen bond to His-163. A trifluoroethanol (FTE) is located close to the ASC. (c) Dithiothreitol (DTT) is observed in monoclinic (C2) crystal form. It does not bind to Cys-41. It rather binds to His-41 forming a sulfenamide. Difference electron density maps shown in (a) - (c) are obtained after refining the 3CLpro without the addition of ligand. The ascorbate and DTT explain the additional electron density.

The Covid-19 pandemic, caused by a novel severe acute respiratory syndrome (SARS) coronavirus 2, has paralyzed public life globally. It has resulted in excess of 500,000 deaths in the US alone as of April 2021. Although potent vaccines are now available, they are optional, not tested in children

35 and potentially not as effective against new viral mutant variants emerging world-wide (LITER).
36 The need for an effective inexpensive treatment and prevention of Covid-19 still exists as large
37 number of infections with potentially severe or lethal outcomes are still reported daily. SARS CoV-
38 2 is a large, enveloped single-stranded RNA betacoronavirus (Cui et al., 2019). The viral RNA
39 encodes two open reading frames that, generates two polyproteins pp1a and pp1ab8. The
40 polyproteins are processed by two viral cysteine proteases: a papain-like protease (PLpro) and a
41 3C-like protease, also referred to as the main protease (Mpro) or 3CLpro, that cleave multiple sites
42 to release non-structural proteins (nsp1-16). These non-structural proteins form the replicase
43 complex responsible for replication and transcription of the viral genome and have led to 3CLpro
44 and PLpro being the primary targets for antiviral drug development. The 3CLpro is a
45 chymotrypsin-like cysteine protease with a Cys/His dyad in the active site (Fig. 1a). The 3C refers
46 to region 3C in the genome of the *picornaviridae* family, where a similar protease is found
47 (Ramajayam et al., 2011). In coronaviruses, the 3CLpro is located in the non-structural protein
48 (NSP) 5 coding region of the virus RNA genome (Wu et al., 2020).
49
50 High throughput structure based drug discovery experiments on 3CL-pro were recently conducted
51 by large groups of scientists at synchrotrons such as Petra III (Gunther et al., 2021), Diamond
52 (Douangamath et al., 2020) and NSLS-II (to be published) among others. This approach was also
53 rapidly deployed after the 2002 SARS-CoV-1 outbreak, with earlier work by the Hilgenfeld group
54 on Mpro (3CLpro) of coronarviruses leading to crystal structures of SARS-CoV-2 Mpro and
55 inhibitor complexes (Zhang, Lin, Kusov, et al., 2020; Zhang, Lin, Sun, et al., 2020). Active sites
56 of coronavirus Mpro are well conserved and those of enteroviruses (3Cpro) are functionally
57 similar: thus, providing an excellent opportunity to develop broad-spectrum antivirals with
58 structural biology approach. However, the most inhibitors investigated so far are marginally water
59 soluble. They have to be added to the crystals in an organic solvent, or they can be co-crystallized.
60 Their relative scarcity, potential toxicity and unspecificity, and a potentially expensive price tag
61 prevents their wide-spread use. Inexpensive, water soluble, and readily available drugs to combat
62 Covid-19 are urgently required.
63
64 Vitamin C has been shown to have antiviral activity for more than half a century, including work
65 of the two-times Nobel Laureate Linus Pauling (Pauling, 1970). Vitamin C is a six-carbon

compound (Scheme 1) and a potent antioxidant. It is available in synthetic form and found naturally in Indian gooseberry, citrus fruits and green leafy vegetables. The revival of interest in Vitamin C therapy for acute inflammatory disorders, grounded in sound biological rationale, follows decades of research. Emerging literature suggests that Vitamin C may also play an adjunctive role in the treatment of a variety of viral infections (Colunga Biancatelli et al., 2020; Fowler Iii et al., 2017). A number of observers including Linus Pauling have suggested in the past that Vitamin C in high dosages is directly virucidal (Furuya et al., 2008; Harakeh et al., 1990; Klein, 1945; Pauling, 1970). This assumption was based on in vitro studies, where very high doses of Vitamin C, in the presence of free copper and/or iron, has virucidal activity, presumably through the generation of hydrogen peroxide and other radical species (Furuya et al., 2008; Klein, 1945).

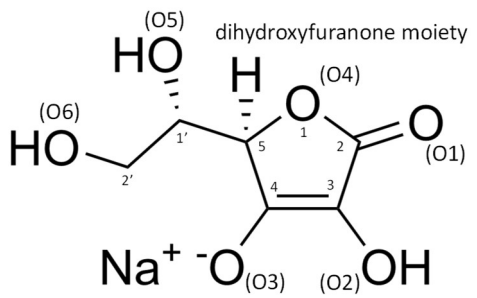

Scheme 1. The chemical structure of sodium L-ascorbate, sodium 5-[(1S)-1,2-dihydroxyethyl]-3-hydroxy-4-oxo-furan-2-olate. The crystallographic annotation of atoms is shown in brackets for oxygens that can be involved in hydrogen bonds.

A recent clinical study of injecting high doses of vitamin-C (> 20 g) intravenously to combat Covid-19 yielded promising results (Zhao et al., 2021). In another study 8 g of Vitamin C was administered orally over three meals together with zinc (Thomas et al., 2021). The results were inconclusive although a positive trend is apparent. So far, it could not be demonstrated that Vitamin C is directly virucidal against Covid-19 *in vivo.*

In order to investigate the binding of Vitamin-C directly to the CoV-2 3CLpro, we co-crystallized CoV-2 3CLpro with low concentrations (5 mmol/L) of L-ascorbate and soaked these crystals before freezing for 3 min in 120 mmol/L ascorbate (Supplementary Material). Difference electron density that can be assigned to ascorbate appears in the active sites near Cys-145 and His-163 of both subunits (Fig. 1). The L-ascorbates only weakly interact with Cys-145 (between 3 Å and 3.7 Å to the sulfur, Tab. 1) but form a tight hydrogen bonding network with Asn-142, Gly-143(N), His-163 and Gln-166 (Fig. S1 and Tab. 1). In addition to the L-ascorbate electron density, an additional density feature is present in the active site. The pillow-like electron density (Fig. 1 b) is interpreted with a trifluoroethanol (FTE) that has been provided as an additive to the crystallization buffer. The interaction of the FTE with the

nearby L-ascorbate is weak as the closest distance is larger than 4 Å (Tab. 1). Fig. 2 compares the L-ascorbate position to the position of compound 13b in the active site of the 3CLpro. Compound 13b is a potent inhibitor of the 3CLpro (Zhang, Lin, Kusov, et al., 2020). The positions of the two compound 13b oxygens O40 and O41 in the 3CLpro are close to the C2' oxygen of the ascorbate (Fig. 2 a). The dihydroxyfuranone ring (Scheme 1) of the ascorbate occupies a similar position as the moiety P1 of compound 13b (Fig. 2 a). The FTE oxygen position is reflected by a structural water found in the compound 13b complexed 3CLpro structure. 3CLpro can also be crystallized in the presence of dithiotreitol (DTT) (Zhang, Lin, Sun, et al., 2020). DTT binds with one of its sulfurs between the Cys-145 and His-41 (Fig. 1 c). As the distance to the His-41 N_e is substantially shorter (1.5 Å) than the one to the Cys-145 sulfur (2.3 Å), the DTT forms a sufenamide with His-41 which is a critical amino acid for the catalytic mechanism of the 3CLpro.

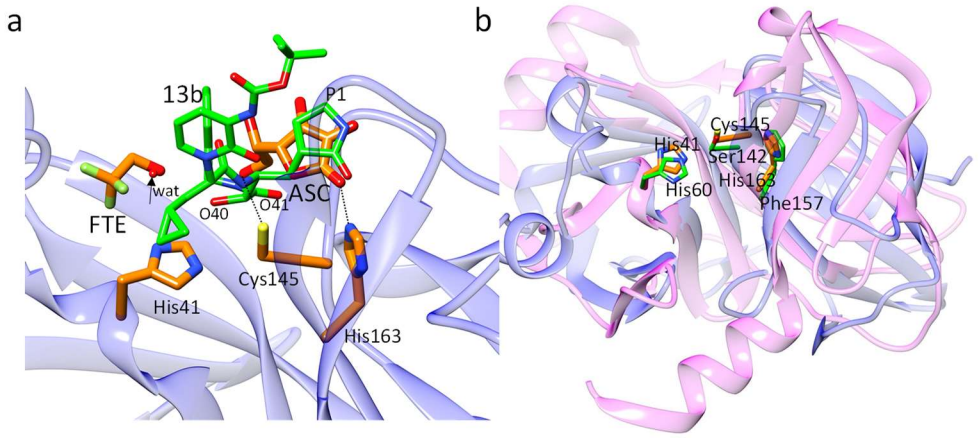

Figure 2. Structural comparisons. **(a)** Comparison of ligands in the active site of CoV-2 3CLpro. The position of the L-ascorbate molecule relative to compound 13b in 3CLpro as determined by Zhang et al., 2020. The positions of the C2'-oxygens is close to the two compound 13b oxygens O40 and O41 (marked), and the dihydroxyfuranone-ring of ASC coincides with the P1 moiety of compound 13b. The arrow points to a water molecule found in the structure of 3CLpro complexed with compound 13b. This position is occupied by the FTE oxygen. **(b)** Overlay of the N-terminal domain of CoV-2 3CLpro (blue ribbon, from residues 8 to 181) on the Hepatitis-C virus (HCV) serine protease (magenta ribbon). Active site residues are shown (orange for the 3CLpro, and green for the HCV protease). The active sites of both proteins are very similar. The positions of the catalytically active Cys145/Ser142 and His41/His60 are essentially identical. His163 in CoV-2 3CLpro is replaced by the structurally similar Phe157 in the HCV protease.

A search for ascorbate in the protein data bank yields 645 protein structures with only 40 structures that have a bound ascorbate. None of the 40 structures are viral proteins. To our knowledge, this is the first structure of a viral protein with ascorbate bound in the active site. The CoV-2 3CLpro has homologues in many other viruses different from coronavirus. As mentioned above, a similar (3C) protease can be found in picornaviruses (Ramajayam et al., 2011). Members of the *picornaviridae* family cause diseases such as polio (poliovirus), encephalomeningitis (encephalomyocarditis virus) and the common cold (rhinovirus) (Sharma & Gupta, 2017). Moreover, the structure of the N-terminal domain of the CoV-2 3CLpro, as well as that of its active site is very similar to the structure of the hepatitis-C virus (HCV) protease (Fig. 2), except that the HCV protease is a serine protease. However, even the HCV protease Ser-142 oxygen position is essentially identical to that of the Cys-145 sulfur in the 3CLpro. The binding of Vitamin C to the CoV-2 3CLpro might point to reasons why Vitamin C could be beneficial for the treatment of coronavirus caused diseases such as SARS and middle east respiratory syndrome (MERS) who have structurally similar 3CLpros (Hilgenfeld, 2014; Zhang, Lin, Sun, et al., 2020). Moreover, Vitamin C might also bind to proteases of other viruses, and assists in the treatment of diseases mentioned above and others such as AIDS (Harakeh et al., 1990), herpes (Furuya et al., 2008; Hoog et al., 1997), rhinovirus induced respiratory distress syndrome (Fowler Iii et al., 2017) and even rabies (Banic, 1975).

Our inhibition test shows that ascorbate inhibits the 3CLpro in the absence of FTE (Fig. 3). This indicates that ascorbate binding to the active site is independent of FTE. L-ascorbate has half maximal inhibitory concentration (IC 50) of about 38 mmol/L (Fig. 3), which is very high compared to other potent inhibitors identified (Gunther et al., 2021; Zhang, Lin, Kusov, et al., 2020) which are all in the µmol/L range. The high IC50 level may explain the sub-stoichiometric ascorbate occupancies (Tab. S1) in both active sites of the 3CLpro. In accordance with the results from our 3CLpro inhibition tests, the effect of ascorbate on viral loads in cell cultures has also been in the millimolar range (Furuya et al., 2008). This might imply that the inhibition of chymotrypsin-like proteases is involved in the virucidal action mechanism. The different results of the clinical studies with Vitamin C (Thomas et al., 2021; Zhao et al., 2021) become explainable in part since the amount of Vitamin C varies from > 20 g administered intravenously to 3 g administered orally per day. Studies have shown that up to 1.5 g Vitamin C per kg body mass can

be safely administered (https://www.cancer.gov/about-cancer/treatment/cam/hp/vitamin-c-pdq). This corresponds to about 10 – 20 mmol/L concentration given a molecular weight of ascorbate of 176 g/mol and the assumption that 45 – 75 % of body mass is water. It may well be that inhibition of proteases with Vitamin C, or perhaps with one of its derivates (Mescic Macan et al., 2019) that

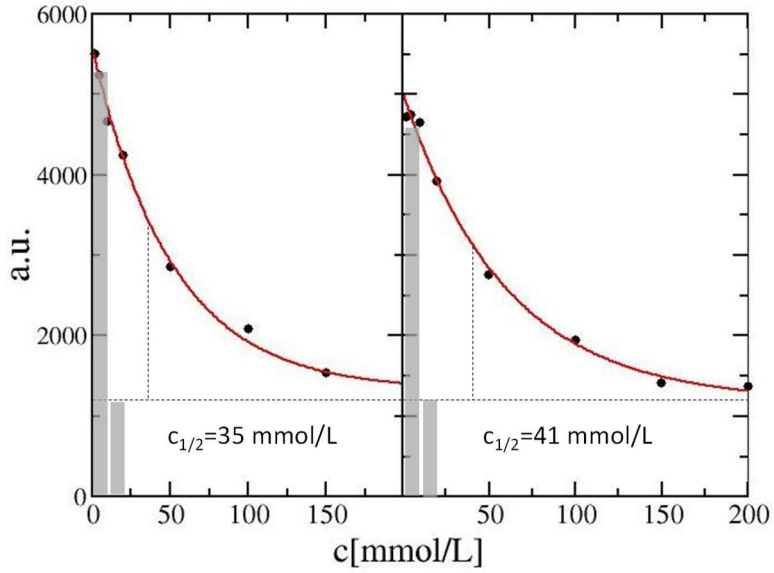

Figure 3. Results from in-vitro inhibition tests of the CoV-2 3CLpro with L-ascorbate. Left panel: 3CLpro as prepared here, right panel: 3CLpro as provided by the 3CLpro inhibition kit. Gray bars: maximum and minimum activities of the 3CLpro. The average $c_{1/2}$ is 38 mmol/L.

may even bind directly to the catalytically important Cys-145, becomes an important factor in the treatment of severe Covid-19 cases and other virus caused infections (Colunga Biancatelli et al., 2020).

149 **Table 1.** Comparison ligand interactions with conserved amino acids in the active site of subunits
150 A and B. Designated atoms of amino acids in subunits A and B and ascorbate ligands that interact
151 are labelled according to annotations in the refined structure (see also Scheme 1).
152

3CLpro / Ascorbate		
	Distances [Å] Subunit A	Distances [Å] Subunit B
Asn142-NOD2 / O5	2.4	2.4
Asn 142-NOD2 / O3	3.2	2.6
Cys145-SG / O6	3.0	3.1
Cys145-SG/ O4	3.7	3.4
His163-NE2 / O1	3.3	2.4
His 163-NE2/O4	3.7	3.9
Glu166-OE2 / O2	3.0	3.0
Gly143-N / O6	2.9	3.1
3CLpro / Trifluoroethanol (FTE)		
His41-ND / F*	3.0	2.9
His41-O / F*	2.8	3.2
CYS44-O / F*	3.0	2.9
Ser 46-OG / O	3.2	4.9
ASC-O6 / O**	4.7	4.6
3CLpro / Dithiothreitol (DTT)		
His41-NE2 / S4	1.4	n.a.***
Cys145-SG / S4	2.6	---
H_2O111-O / S1	2.6	---

153 *shortest to any of the three flour atoms
154 ** shortest FTE to Ascorbate distance
155 **only one subunit in the asymmetric unit
156
157

158 **Supplementary Material**

159

160 *Expression.* The CoV-2 3CLpro sequence was synthetized (GenScript) for optimized expression
161 in E. coli according to sequence information published previously(Zhang, Lin, Sun, et al., 2020).
162 In short, the N-terminus of 3CLpro is fused to glutathione-S-transferase (GST). It further has a 6-
163 His tag at the c-terminus. The N-terminal GST will be autocatalytically cleaved off after expression
164 due to an engineered 3CLpro cleavage sequence. Although the His tag can be cleaved off by a
165 PreScission protease, the tag did not interfere with crystallization and consequently was left on.
166 Overexpression and protein purification protocols were modified from previous reports. E. coli
167 were grown to 0.8 OD_{600} at 37º in terrific broth. Expression was induced by 1 mmol/L IPTG at 25º
168 C. After 3 h of expression, the culture was induced a second time (1 mmol/L IPTG), and shaken
169 overnight at 20º C. The yield is about 80 mg for a 6 L culture. Cells were resuspended in lysis
170 buffer (20mM Tris Base, 150 mmol/L NaCl, pH 7.8.). After lysis of the bacterial cells, debris was
171 centrifuged at 50,000 g for 1 hour. The lysate was let stand at room temperature for 3 h (overnight
172 is also possible). After this, the lysate was pumped through a column containing 15 mL of Talon
173 Cobalt resin (TAKARA). The resin was washed without using imidazole using a wash cycle
174 consisting of low salt (20 mmol/L Tris Base, 50 mmol/L NaCl, pH 7.8), high salt (20 mmol/L Tris
175 Base, 1 mol/L NaCl, pH 7.8) and low salt (as above) solutions (about 20 column volumes each).
176 After the wash cycle was completed, the column was let stand for an additional 2 h at room
177 temperature followed by another wash cycle. The final product was eluted by 300 mmol/L
178 imidazole. Buffer exchange was achieved at 4 º C by either by 3 times spin-concentration and re-
179 dilution with 20 mmol/L Tris base, 150 mmol/L NaCl, 25 mmol/L Na-ascorbate, or by dialyzing
180 immediately in 20 mmol/L Tris base, 150 mmol/L NaCl, 0.1 mmol/L dithiotreitol (DTT), pH 7.8.
181 The preparations were concentrated to a 3CLpro concentration of 20 mg/mL. Since the 6-His tag
182 was not cleaved off, this one step purification protocol required only ~10 h from cell lysis to the
183 pure 3CLpro product. The product is within 1.7 Da of the theoretical molecular weight as
184 determined by mass spectroscopy.

185

186 *Crystallization.* The concentrated 3CLpro containing DTT was diluted to 4 mg/mL. 100 µL of the
187 diluted 3CLpro was mixed (1:1) in batch mode with the same amount of 25 % PEG 3350, Bis-Tris
188 100 mmol/L, pH 6.5. Rectangular shaped crystals with dimensions of about 200 x 30 x 30 μm^3

189 were obtained. Crystals of the ascorbate containing 3CLpro were obtained by the hanging drop
190 method by mixing 2 µL of 30 mg/mL protease with an equal amount of a reservoir solution
191 containing 15 % PEG 3350, 5 mmol/L ascorbate, and trifluoroethanol (FTE) (4 %) as an additive.
192 Crystals formed long thin needles after 3-day incubation at 16° C. Crystals were soaked in mother
193 liquor containing an addition of 120 mmol/L ascorbate and 20 % glycerol as a cryoprotectant for
194 3 min before freezing.
195
196 *Data Collection and Structure determination.* The crystals were mounted in Mitegen micro-loops
197 (30 - 50 µm) and directly frozen in pucks suspended in liquid nitrogen for automated (robotic) data
198 collection. The dewar with the pucks were provided to the Advanced Photon Source, Argonne
199 National Lab, Lemont, IL, for robotic data collection at Sector-19 (Structural Biology Center,
200 SBC, beamline 19-ID-D). Data collection was fully remote due to restriction of the COVID-19
201 pandemic. Dataset to 2.2 Å and 2.5 Å, respectively, were collected (0.5° rotation and 0.8 s exposure
202 per detector readout for a total of 180°) on the 3CLpro with DTT and L-ascorbate, respectively.
203 Data was processed with HKL3000 (Minor et al., 2006). Data statistics in shown in Tab. 1. The
204 spacegroup of the DTT containing crystals was C2. For refinement, the 3CLpro structure with pdb
205 access code 6Y2E (Zhang, Lin, Sun, et al., 2020) was used as initial model. Molecular replacement
206 was not necessary as the model fits immediately. Refinement was achieved using refmac
207 (Murshudov et al., 2011) (version 5.8.0238). The electron density of the DTT becomes apparent
208 by a difference electron density feature in between His-41 and Cys-145 (Fig. 1 c). With L-
209 ascorbate and FTE in the buffer, the spacegroup becomes $P2_12_12_1$ with cell constants not found so
210 far for the CoV-2 3CLpro. Molecular replacement was performed by Phaser (Oeffner et al., 2013)
211 version 2.8.2 using pdb-entry 6XQT (Kneller et al., 2020) as a search model. After refinement of
212 the molecular replacement solution, difference electron density of both, the L-ascorbate and the
213 FTE becomes apparent in the active sites of both subunits (Fig. 1 a). The positions and orientations
214 of the L-ascorbates and the FTE molecules were determined with the help of Polder maps (Fig. 1a
215 and b) (Liebschner et al., 2017) calculated using Phenix (Adams et al., 2010) v1.19.2-4158. After
216 conventional refinement in Phenix, grouped occupancy refinement resulted in sub-stochiometric
217 concentrations with occupancy values of the L-ascorbates varying from ~60 % in subunit A to ~70
218 % in subunit B.
219

220 *In-vitro 3CLpro enzyme activity test.* The 3CLpro activity was tested using the 'Untagged (SARS-
221 CoV-2) Assay Kit' (BPS Biosciences). The L-ascorbate concentration was varied from 0.2
222 mmol/L to 200 mmol/L. Trifluoroethanol (which has been used as an additive in the crystallization
223 trails) was not added. High concentration of ascorbate has neither an effect on the fluorescence of
224 the substrate nor on the stability of the 3CLpro (not shown). Half inhibition (IC50) of the 3CLpro
225 is observed at 38 mmol/L (Fig. S1).
226
227

Table S1. Data collection and refinement statistics.

	SARS CoV-2 3CLpro	
Beamline	APS 19-ID-D	
Temperature	110 K	
Ligand	L-ascorbate (Vitamin C)	Dithiothreitol (DTT)
Resolution (Å)	2.3	2.3
Space group	$P2_12_12_1$	C2
Unit-cell parameters (Å,°)	a = 65.4 Å b = 67.5 Å c= 157.5 Å α=90° β=90° γ=90°	a = 113.39 Å b = 53.4 Å c= 44.7 Å α=90° β=102.8° γ=90°
No of unique reflections	30845	9426
Redundancy	5.7 (3.9)	3.1 (1.8)
Completeness (%)	98.2 (90.0)	70.0
CC1/2 @ dmin	45.2	47.6
R_{merge} (%)	20.4 (145.6)	7.3 (122)
Model Building/ Refinement	Phenix 1.19.2-4158 to 2.3 Å	refmac 5.8.0258 to 2.2 Å
R_{cryst}/R_{free} (%)	21.0/24.4	19.1/26.3
# subunit/asymmetric unit	2	1
# residues/subunit	303/310*	303
additional ligand	trifluoroethanol (FTE)	n.o.
ligand occupancy	Vitamin C: A 0.66; B 0.67** FTE: A 0.66; B: 0.68	0.85
# water	198	1184
R.m.s.d. bonds (Å)/angles (°)	0.005/1.07	0.007/0.949
Coordinate Error (Å)	0.25	0.18

*in subunit B, electron density for seven additional C-terminal residues including that of two histidines of the hexa-his tag can be observed.

**the difference electron density in any F^{obs}-F^{calc} difference map including the Polder map is visually weaker in the active site of subunit A compared to that of subunit B.

n.o.: no additional ligand

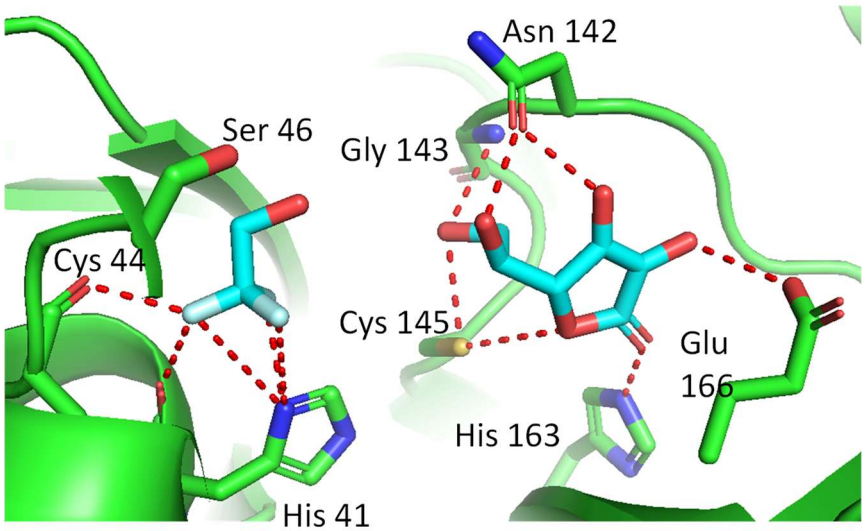

Figure S1. Interaction pattern of the L-ascorbate and FTE with the active site of 3CLpro subunit B. The pattern is very similar in subunit A.

237
238 **References**
239

240 Adams, P. D., Afonine, P. V., Bunkoczi, G., Chen, V. B., Davis, I. W., Echols, N., Headd, J. J., Hung,
241 L. W., Kapral, G. J., Grosse-Kunstleve, R. W., McCoy, A. J., Moriarty, N. W., Oeffner, R.,
242 Read, R. J., Richardson, D. C., Richardson, J. S., Terwilliger, T. C., & Zwart, P. H. (2010).
243 PHENIX: a comprehensive Python-based system for macromolecular structure solution.
244 *Acta Crystallogr D Biol Crystallogr*, *66*(Pt 2), 213-221.
245 https://doi.org/10.1107/S0907444909052925
246 Banic, S. (1975). Prevention of Rabies by Vitamin C. *Nature*, *258*, 2.
247 Colunga Biancatelli, R. M. L., Berrill, M., & Marik, P. E. (2020). The antiviral properties of vitamin
248 C. *Expert Rev Anti Infect Ther*, *18*(2), 99-101.
249 https://doi.org/10.1080/14787210.2020.1706483
250 Cui, J., Li, F., & Shi, Z. L. (2019). Origin and evolution of pathogenic coronaviruses. *Nature Reviews*
251 *Microbiology*, *17*(3), 181-192. https://doi.org/10.1038/s41579-018-0118-9
252 Douangamath, A., Fearon, D., Gehrtz, P., Krojer, T., Lukacik, P., Owen, C. D., Resnick, E., Strain-
253 Damerell, C., Aimon, A., Abranyi-Balogh, P., Brandao-Neto, J., Carbery, A., Davison, G.,
254 Dias, A., Downes, T. D., Dunnett, L., Fairhead, M., Firth, J. D., Jones, S. P., Keeley, A.,
255 Keseru, G. M., Klein, H. F., Martin, M. P., Noble, M. E. M., O'Brien, P., Powell, A., Reddi, R.
256 N., Skyner, R., Snee, M., Waring, M. J., Wild, C., London, N., von Delft, F., & Walsh, M. A.
257 (2020). Crystallographic and electrophilic fragment screening of the SARS-CoV-2 main
258 protease. *Nature Communications*, *11*(1), 5047. https://doi.org/10.1038/s41467-020-
259 18709-w
260 Fowler Iii, A. A., Kim, C., Lepler, L., Malhotra, R., Debesa, O., Natarajan, R., Fisher, B. J., Syed, A.,
261 DeWilde, C., Priday, A., & Kasirajan, V. (2017). Intravenous vitamin C as adjunctive therapy
262 for enterovirus/rhinovirus induced acute respiratory distress syndrome. *World J Crit Care*
263 *Med*, *6*(1), 85-90. https://doi.org/10.5492/wjccm.v6.i1.85
264 Furuya, A., Uozaki, M., Yamasaki, H., Arakawa, T., Arita, M., & Koyama, A. H. (2008). Antiviral
265 effects of ascorbic and dehydroascorbic acids in vitro. *Int J Mol Med*, *22*(4), 541-545.
266 https://www.ncbi.nlm.nih.gov/pubmed/18813862
267 Gunther, S., Reinke, P. Y. A., Fernandez-Garcia, Y., Lieske, J., Lane, T. J., Ginn, H. M., Koua, F. H.
268 M., Ehrt, C., Ewert, W., Oberthuer, D., Yefanov, O., Meier, S., Lorenzen, K., Krichel, B.,
269 Kopicki, J. D., Gelisio, L., Brehm, W., Dunkel, I., Seychell, B., Gieseler, H., Norton-Baker, B.,
270 Escudero-Perez, B., Domaracky, M., Saouane, S., Tolstikova, A., White, T. A., Hanle, A.,
271 Groessler, M., Fleckenstein, H., Trost, F., Galchenkova, M., Gevorkov, Y., Li, C., Awel, S.,
272 Peck, A., Barthelmess, M., Schluenzen, F., Lourdu Xavier, P., Werner, N., Andaleeb, H.,
273 Ullah, N., Falke, S., Srinivasan, V., Franca, B. A., Schwinzer, M., Brognaro, H., Rogers, C.,
274 Melo, D., Zaitseva-Doyle, J. J., Knoska, J., Pena-Murillo, G. E., Mashhour, A. R., Hennicke,
275 V., Fischer, P., Hakanpaa, J., Meyer, J., Gribbon, P., Ellinger, B., Kuzikov, M., Wolf, M.,
276 Beccari, A. R., Bourenkov, G., von Stetten, D., Pompidor, G., Bento, I., Panneerselvam, S.,
277 Karpics, I., Schneider, T. R., Garcia-Alai, M. M., Niebling, S., Gunther, C., Schmidt, C.,
278 Schubert, R., Han, H., Boger, J., Monteiro, D. C. F., Zhang, L., Sun, X., Pletzer-Zelgert, J.,
279 Wollenhaupt, J., Feiler, C. G., Weiss, M. S., Schulz, E. C., Mehrabi, P., Karnicar, K., Usenik,
280 A., Loboda, J., Tidow, H., Chari, A., Hilgenfeld, R., Uetrecht, C., Cox, R., Zaliani, A., Beck, T.,

281 Rarey, M., Gunther, S., Turk, D., Hinrichs, W., Chapman, H. N., Pearson, A. R., Betzel, C., &
282 Meents, A. (2021). X-ray screening identifies active site and allosteric inhibitors of SARS-
283 CoV-2 main protease. *Science*. https://doi.org/10.1126/science.abf7945
284 Harakeh, S., Jariwalla, R. J., & Pauling, L. (1990). Suppression of Human-Immunodeficiency-Virus
285 Replication by Ascorbate in Chronically and Acutely Infected-Cells. *Proc Natl Acad Sci U S*
286 *A*, *87*(18), 7245-7249. https://doi.org/DOI 10.1073/pnas.87.18.7245
287 Hilgenfeld, R. (2014). From SARS to MERS: crystallographic studies on coronaviral proteases
288 enable antiviral drug design. *Febs Journal*, *281*(18), 4085-4096.
289 https://doi.org/10.1111/febs.12936
290 Hoog, S. S., Smith, W. W., Qiu, X., Janson, C. A., Hellmig, B., McQueney, M. S., O'Donnell, K.,
291 O'Shannessy, D., DiLella, A. G., Debouck, C., & Abdel-Meguid, S. S. (1997). Active site cavity
292 of herpesvirus proteases revealed by the crystal structure of herpes simplex virus
293 protease/inhibitor complex. *Biochemistry*, *36*(46), 14023-14029.
294 https://doi.org/10.1021/bi9712697
295 Klein, M. (1945). The Mechanism of the Virucidal Action of Ascorbic Acid. *Science*, *101*(2632),
296 587-589. https://doi.org/10.1126/science.101.2632.587
297 Kneller, D. W., Galanie, S., Phillips, G., O'Neill, H. M., Coates, L., & Kovalevsky, A. (2020).
298 Malleability of the SARS-CoV-2 3CL M(pro) Active-Site Cavity Facilitates Binding of Clinical
299 Antivirals. *Structure*, *28*(12), 1313-1320 e1313. https://doi.org/10.1016/j.str.2020.10.007
300 Liebschner, D., Afonine, P. V., Moriarty, N. W., Poon, B. K., Sobolev, O. V., Terwilliger, T. C., &
301 Adams, P. D. (2017). Polder maps: improving OMIT maps by excluding bulk solvent. *Acta*
302 *Crystallogr D Struct Biol*, *73*(Pt 2), 148-157. https://doi.org/10.1107/S2059798316018210
303 Mescic Macan, A., Gazivoda Kraljevic, T., & Raic-Malic, S. (2019). Therapeutic Perspective of
304 Vitamin C and Its Derivatives. *Antioxidants (Basel)*, *8*(8).
305 https://doi.org/10.3390/antiox8080247
306 Minor, W., Cymborowski, M., Otwinowski, Z., & Chruszcz, M. (2006). HKL-3000: the integration
307 of data reduction and structure solution - from diffraction images to an initial model in
308 minutes. *Acta Crystallographica Section D-Structural Biology*, *62*, 859-866. <Go to
309 ISI>://WOS:000239119800003
310 Murshudov, G. N., Skubak, P., Lebedev, A. A., Pannu, N. S., Steiner, R. A., Nicholls, R. A., Winn, M.
311 D., Long, F., & Vagin, A. A. (2011). REFMAC5 for the refinement of macromolecular crystal
312 structures. *Acta Crystallogr D Biol Crystallogr*, *67*(Pt 4), 355-367.
313 https://doi.org/10.1107/S0907444911001314
314 Oeffner, R. D., Bunkoczi, G., McCoy, A. J., & Read, R. J. (2013). Improved estimates of coordinate
315 error for molecular replacement. *Acta Crystallographica Section D-Biological*
316 *Crystallography*, *69*, 2209-2215. https://doi.org/Doi 10.1107/S0907444913023512
317 Pauling, L. (1970). *Vitamin C and the Common Cold*. W. H. Freeman and Company.
318 Ramajayam, R., Tan, K. P., & Liang, P. H. (2011). Recent development of 3C and 3CL protease
319 inhibitors for anti-coronavirus and anti-picornavirus drug discovery. *Biochem Soc Trans*,
320 *39*(5), 1371-1375. https://doi.org/10.1042/BST0391371
321 Sharma, A., & Gupta, S. P. (2017). Fundamentals of Viruses and Their Proteases. *Viral Proteases*
322 *and Their Inhibitors*, 1-24. https://doi.org/10.1016/B978-0-12-809712-0.00001-0
323 Thomas, S., Patel, D., Bittel, B., Wolski, K., Wang, Q., Kumar, A., Il'Giovine, Z. J., Mehra, R.,
324 McWilliams, C., Nissen, S. E., & Desai, M. Y. (2021). Effect of High-Dose Zinc and Ascorbic

325 Acid Supplementation vs Usual Care on Symptom Length and Reduction Among
326 Ambulatory Patients With SARS-CoV-2 Infection: The COVID A to Z Randomized Clinical
327 Trial. *JAMA Netw Open*, *4*(2), e210369.
328 https://doi.org/10.1001/jamanetworkopen.2021.0369
329 Wu, F., Zhao, S., Yu, B., Chen, Y.-M., Wang, W., Song, Z.-G., Hu, Y., Tao, Z.-W., Tian, J.-H., Pei, Y.-
330 Y., Yuan, M.-L., Zhang, Y.-L., Dai, F.-H., Liu, Y., Wang, Q.-M., Zheng, J.-J., Xu, L., Holmes, E.
331 C., & Zhang, Y.-Z. (2020). A new coronavirus associated with human respiratory disease in
332 China. *Nature*, *579*, 4. https://doi.org/https://doi.org/10.1038/s41586-020-2008-3
333 Zhang, L. L., Lin, D. Z., Kusov, Y., Nian, Y., Ma, Q. J., Wang, J., von Brunn, A., Leyssen, P., Lanko, K.,
334 Neyts, J., de Wilde, A., Snijder, E. J., Liu, H., & Hilgenfeld, R. (2020). alpha-Ketoamides as
335 Broad-Spectrum Inhibitors of Coronavirus and Enterovirus Replication: Structure-Based
336 Design, Synthesis, and Activity Assessment. *Journal of Medicinal Chemistry*, *63*(9), 4562-
337 4578. <Go to ISI>://WOS:000535279800012
338 Zhang, L. L., Lin, D. Z., Sun, X. Y. Y., Curth, U., Drosten, C., Sauerhering, L., Becker, S., Rox, K., &
339 Hilgenfeld, R. (2020). Crystal structure of SARS-CoV-2 main protease provides a basis for
340 design of improved alpha-ketoamide inhibitors. *Science*, *368*(6489), 409-+. <Go to
341 ISI>://WOS:000528513300041
342 Zhao, B., Ling, Y., Li, J., Peng, Y. B., Huang, J., Wang, Y. H., Qu, H. P., Gao, Y., Li, Y. C., Hu, B. J., Lu,
343 S. H., Lu, H. Z., Zhang, W. H., & Mao, E. Q. (2021). Beneficial aspects of high dose
344 intravenous vitamin C on patients with COVID-19 pneumonia in severe condition: a
345 retrospective case series study. *Annals of Palliative Medicine*, *10*(2), 1599-+.
346 https://doi.org/10.21037/apm-20-1387
347